

# Graphite intercalation compound $\text{KC}_8$ revisited: a key to graphene

A. Grüneis<sup>1</sup>, C. Attaccalite<sup>2</sup>, A. Rubio<sup>2</sup>, D. Vyalikh<sup>3</sup>, S.L. Molodtsov<sup>3</sup>, J. Fink<sup>4</sup>, R. Follath<sup>4</sup>,  
W. Eberhardt<sup>4</sup>, B. Büchner<sup>1</sup>, T. Pichler<sup>5</sup>

<sup>1</sup>*IFW Dresden, P.O. Box 270116, D-01171 Dresden, Germany*

<sup>2</sup>*Nano-Bio Spectroscopy Group and European Theoretical Spectroscopy Facility (ETSF), Departamento de Física de Materiales, Unidad de Materiales Centro Mixto CSIC-UPV/EHU, Universidad del País Vasco, Avd. Tolosa 72, E-20018 Donostia, Spain*

<sup>3</sup>*Institut für Festkörperphysik, TU Dresden, Mommsenstrasse 13, D-01069 Dresden, Germany*

<sup>4</sup>*BESSY II, Albert-Einstein-Str. 15, D-12489 Berlin, Germany*

<sup>5</sup>*Faculty of Physics, University of Vienna, Boltzmanngasse 5, A-1090 Vienna, Austria*

**Electrons in isolated graphene layers are a two-dimensional gas of massless Dirac Fermions. In realistic devices, however, the electronic properties are modified by elastic deformations, interlayer coupling and substrate interaction. Here we unravel the electronic structure of doped graphene, revisiting the stage one graphite intercalation compound  $\text{KC}_8$  using angle-resolved photoemission spectroscopy and ab-initio calculations. The full experimental dispersion is in excellent agreement to calculations of doped graphene once electron correlations are included on the  $GW$  level. This highlights that  $\text{KC}_8$  has negligible interlayer coupling. Therefore Dirac Fermion behaviour is preserved and we directly determine the full experimental Dirac cone of doped graphene. In addition we prove that superconductivity in  $\text{KC}_8$  is**

**mediated by electron–phonon coupling to an iTO phonon, yielding a strong kink in the quasi-particle dispersion at 166 meV. These results are key for understanding, both, the unique electronic properties of graphene and superconductivity in  $\text{KC}_8$ .**

The recent discovery of two–dimensional meta–stable graphene sheets has sparked enormous interest in their low–energy electronic structure <sup>1–4</sup>. Graphene samples are in general obtained by three methods: (1) repeated peeling of a graphite single crystal <sup>3</sup>, (2) growth by chemical vapour deposition on Ni(111) <sup>5,6</sup> and (3) precipitating few–layer graphene from SiC <sup>7</sup>. Angle–resolved photoemission spectroscopy (ARPES) has been proven to be a key tool to determine the electronic structure of one and few layer graphene <sup>8</sup> and graphite <sup>4,9,10</sup>. A major problem for the investigation of substrate based graphene is that there is a significant modification of the electronic structure due to interaction with the substrates yielding charge transfer and hybridisation <sup>6</sup>.

One way to overcome this problem is to measure single crystalline graphite, which has no substrate interaction. In this case however, a  $k_z$  dispersion of two  $\pi$  valence bands <sup>9</sup> and a small gap <sup>11</sup> were observed because of the AB stacking sequence of graphene layers. Another important issue in both systems is the renormalization of the bare electronic band structure due to doping dependent electron–electron correlation <sup>9</sup>, electron–phonon coupling (EPC) <sup>10,12</sup> or electron–plasmon coupling <sup>13</sup>.

In order to circumvent the problems of substrate interaction, strong bilayer splitting and electron–electron correlation we revisited stage one graphite intercalation compound (GIC)  $\text{KC}_8$ . GICs have been at the focus of intense research in the last four decades because they have a wide

range of tunable electronic properties<sup>14</sup>. Especially, for stage I GICs superconductivity was observed with transition temperatures  $T_C$  ranging from below 1 K for alkali metal intercalation (e.g. 0.55 K for  $\text{KC}_8$ <sup>15</sup>) up to 11.5 K for  $\text{CaC}_6$ <sup>16</sup>. In both cases EPC is the superconducting pairing mechanism<sup>16–18</sup>. In stage I alkali GICs the graphene layers have *AA* stacking and only one  $\pi$  conduction(valence) band and can thus be considered as a doped graphene layer sandwiched in between two positively charged plates (Supplementary Fig. S1). Thus the low-energy band structure of, both, stage I GICs and graphene are described by a  $2 \times 2$  tight-binding (TB) Hamiltonian<sup>19,20</sup> resulting in a linear  $\pi$  band dispersion close to the crossing point of the valence and conduction bands. The electronic band structure of GICs was also calculated by density functional theory in the local density approximation (LDA)<sup>21</sup>. Experimentally, preliminary studies on ARPES of GICs were reported<sup>22,23</sup>. Until now the details in the low energy quasiparticle (QP) dispersion of GICs regarding the superconducting coupling mechanism are not identified. Furthermore the issue of whether the charge transfer to graphite is complete<sup>24–27</sup> or partial<sup>22,23,28</sup> was never resolved.

In this work we revisited the electronic structure of  $\text{KC}_8$  GICs using a combination of ARPES and ab-initio calculations. We proof a complete charge transfer and find excellent agreement to ab-initio *GW* calculations including electron–electron correlation. This highlight that a rigid band shift model of graphene is applicable for  $\text{KC}_8$  and electron–electron correlation play a crucial role in the QP dispersion. Hence we unravel for the first time the full experimental Dirac cone of graphene without modifications by substrate interactions and directly determine the corresponding momentum dependent Fermi velocities ( $v_F$ ) in the valence and conduction bands. Thus our results are key for understanding the unique doping dependent electronic transport properties of gated

graphene layers in nanoelectronic devices. In addition we show a detailed study of the direction dependent renormalization of the QP dispersion at low binding energy that highlights the coupling to an iTO phonon at 166 meV. We directly show that the coupling to this phonon, which is also responsible for the double–resonance Raman process, is the major contribution to the superconducting pairing in  $\text{KC}_8$ .

The  $\text{KC}_8$  crystal structure is given by individual graphene sheets separated by layers of potassium as shown in Fig. 1(a). This compound was synthesized in–situ by evaporation of potassium as described in detail in the Methods section. The fully intercalated graphite crystals have a characteristic golden colour as shown in Fig. 1(b). We now carry out a detailed analysis of the QP dispersion of  $\text{KC}_8$  as measured by ARPES. In Fig. 1(c) we show energy dispersion curves (EDC) and cuts of the  $\pi$  bands that intersect the corners of the Brillouin zone (BZ). The cuts are done close to the  $k_y$  direction [see coordinate system in Fig. 4(b)]. We also measured the photon energy dependence and, beside changes in the matrix elements, do not observe a dispersion perpendicular to the layers. Fig. 1(d) shows equi–energy cuts of the raw photoemission intensity. When moving from the cut at  $E_F$  to lower energies the circumference of the equi–energy contour of the conduction band becomes smaller. Evidently we have one  $\pi$  valence and one  $\pi$  conduction band and they meet in one point. Therefore in akin analogy to graphene the crossing point at 1.35 eV is from now on called the ”Dirac point”. Decreasing the energy of the cut below 1.35 eV enlarges the equi–energy contour of the valence band. Comparing two contours with the same distance from the Dirac point [e.g. cuts at  $E_F$  and 2.7 eV in Fig. 1(d)], it can be seen that the  $\pi$  valence band is steeper and has less trigonal warping. Such a result is related to the fact that the self–energy corrections to the

trigonal warping effect increase with doping<sup>29</sup>. Interestingly, as depicted in Fig. 1(d), the photoemission matrix elements of the valence and conduction bands are complementary yielding a high photoemission intensity in 1/3 and 2/3 of the BZ, respectively. From the contour at  $E_F$  in Fig. 1(d) we determine the number of carriers  $n_e$  by integrating the volume inside the Fermi surface. This yields  $n_e = 7.2 \times 10^{21}$  electrons  $\text{cm}^{-3}$ , close to a full charge transfer ( $n_e = 8.9 \times 10^{21}$  electrons  $\text{cm}^{-3}$ ). The remaining deviations can be explained by a slightly lower stoichiometry, i.e.  $\text{K}_{0.85}\text{C}_8$ . From these results, concomitant with the absence of any Fermi surface of K 4s states close to the  $\Gamma$  point (Supplementary Fig. S7) we can safely state a complete charge transfer from potassium in agreement with previous results<sup>24–27</sup>. As can be seen in Fig. 2 the ARPES intensity maxima at  $E_F$  and the linear dispersion close to the Dirac point are very well described by a TB fit including third nearest neighbours (NN) (Supplementary Table 1). First NN TB calculations are inadequate and can not describe the experimental equi-energy contours. This new TB fit reproduces very well the experiments shown in Fig. 2 and will be also used for the self-energy analysis of the EPC to be described below.

In order to further understand the underlying band structure on an ab-initio level we compared the experimental results to calculations at six different levels comprising LDA and  $GW$ <sup>30–32</sup> calculations of (un)doped graphene and  $\text{KC}_8$ . As seen in the Supplementary in Fig. S2-S6, band structures calculated at the level of LDA are too flat yielding an incomplete charge transfer with a partially occupied K 4s band in the vicinity of the  $\Gamma$  point. Calculations on the  $GW$  level including full and partial self consistency in G are in much better agreement to the experiment. The obtained results for the QP dispersion at  $K$  are identical but only the latter explains the lack of pho-

photoemission intensity at the  $\Gamma$  point in  $\text{KC}_8$  (Supplementary Figs. S7-S8). As depicted in Fig. 2(a) the observed linear dispersion is reminiscent of the underlying structure of the graphene parent compound and in perfect agreement to the  $GW$  calculations of graphene. This also holds for the equi-energy contour of the photoemission intensity at  $E_F$  shown in Fig. 2(b). These results clearly indicate that electron-electron correlation is crucial to explain the size of the Fermi surface and the observed trigonal warping. I.e. electron-electron correlation is at the heart of the band structure of the underlying (doped) graphene layers. Hence our results unambiguously highlight the following facts inherent to the electronic structure of doped graphene without substrate interaction: (i) the shape of the Dirac Fermions depends on the doping level and the equi-energy contours above and below the Dirac point are anisotropic; (ii) the trigonal warping increases as doping increases; (iii) in  $\text{KC}_8$  each potassium atom transfers one electron to the graphene layers.

Most importantly let us now turn to a quantitative assessment of the QP bandstructure around the Dirac point, i.e. unravelling for the first time the full experimental Dirac cone. For this purpose, we extracted the photoemission maxima for binding energies between  $E_F$  and 3 eV in steps of 10 meV. The results are depicted in Fig. 3(a). It is obvious that the two-dimensional band structure close to the Dirac point is linear and two bands meet each other in one point. This highlights that  $\text{KC}_8$  indeed consists of doped sheets of graphene and can be well described with the aforementioned TB and  $GW$  approaches. We point out that this is in contrast to all previous experiments on substrate based graphene, clearly observing the opening of a gap in the electronic structure of epitaxial graphene on  $\text{Ni}(111)$  <sup>6</sup> and  $\text{SiC}$  <sup>33</sup>. Although the origin of the gap in graphene on  $\text{SiC}$  is under debate <sup>34</sup> its existence is accepted. The opening of a gap causes a breakdown of Dirac

Fermions which has profound limitation on the observation of relativistic physics in graphene. Therefore the spectroscopic investigation of doped graphene layers in  $\text{KC}_8$  provides an elegant solution to this problem.

Hence, by analyzing the full two-dimensional dispersion of  $\text{KC}_8$  around the Dirac point we can thus actually learn about the physics of graphene. In order to further underline the validity of this analogy we analyze the experimental direction dependent  $v_F$  in the region of 0.1 eV above and below the Dirac point. These results for the valence and conduction band along with the  $GW$  calculations of doped graphene are depicted in Fig. 3(b) and Fig. 3(c), respectively. The  $v_F$  has a maximum(minimum) in  $KT(KM)$  direction. The very good quantitative agreement highlights the validity of our approach. In close similarity to our results on pristine graphite<sup>9</sup>, we observed that electron–electron correlation is crucial to explain the band structure of doped graphene layers in  $\text{KC}_8$ .

We now turn to the analysis of QP bandstructure of  $\text{KC}_8$  close to  $E_F$  and their implications for superconductivity. In addition to the linear dispersion, as can be see in Fig. 1(c) Fig. 2(a) and Fig. 3(a), the  $\pi$  conduction band of  $\text{KC}_8$  is strongly kinked at 166 meV. This is in agreement to previous results on doped graphene<sup>12</sup>. By an accurate comparision to the graphite phonon dispersion relation<sup>35–37</sup> we can unambiguously assign the kink to a coupling to the in–plane transverse optical (iTO) phonon branch near the  $K$  point (see the Supplementary Table 2 for the calculated phonon frequencies including non-adiabatic effects). This agrees perfectly with both the energy of the kink and also with the facts that the EPC matrix element with the iTO phonons is much stronger

than with  $\Gamma$  point phonons<sup>38</sup> and that the phonon density of states is strongly peaked due to the flat dispersion of the iTO branch around  $K$ . The photohole decay process is shown schematically in Fig. 4(a). It is clear that a photohole can relax to a lower binding energy state in two ways by intravalley and intervalley scattering. For the case of intravalley scattering the photohole scatters around  $K$  or  $K'$  points and relaxes by emission of  $\Gamma$  point phonons. However, as their energy does not fit with the measured kink we disregard this mechanism. Therefore the relevant process is related to intervalley scattering where the photohole scatters between  $K$  and  $K'$  points and relaxes by emitting phonons close to the  $K$  point. In Fig. 4(b) we illustrate this mechanism in the 2D BZ of graphene with the exchange of a phonon with wavevector  $q_{ph}$ . Interestingly, a very similar process for scattering of photoexcited electrons is responsible for the  $D$  and  $G'$  band in the double resonance Raman process in  $sp^2$  hybridized carbon materials.

Once we have identified the phonon mode responsible for the observed kink it is important to accurately determine  $\lambda$ , the EPC constant<sup>39</sup>. In recent works<sup>12,40</sup>  $\lambda$  was estimated from the change in the slope of linear bare electronic bands; however this is not justified as the proper bare band structure at the  $E_F$  has to be considered, as was clearly pointed out in a recent theoretical work<sup>41</sup>. In the present work we avoid this problem by considering the total self-energy  $\Sigma(E)$  from which  $\lambda$  can be directly obtained by a simple energy derivative at  $E_F$   $\lambda = -\frac{\partial \text{Re}(\Sigma(E))}{\partial E}|_{E=E_F}$ . To do so we fit the momentum distribution curves (MDCs) of the QP band structure by Lorentzians. The positions of the maxima and the widths of the MDCs are directly proportional to the real and imaginary part of  $\Sigma$ , i.e.  $\text{Re}(\Sigma)$  and  $\text{Im}(\Sigma)$ , respectively (see Supplementary Figs. 9-10). The QP dispersion in the energy region close to the kink is shown in detail in Fig. 4(c) along with the measured maxima of



MDCs and the bare band dispersion (the cut is in  $k_y$  direction in between  $KM$  and  $K\Gamma$  and thus corresponds to an averaged  $\lambda$ ). In the simple case of coupling to one Einstein phonon  $\text{Re}(\Sigma)$  has a peak and  $\text{Im}(\Sigma)$  has a jump at the energy of the coupling phonon mode<sup>39</sup>. Indeed this is what we observe in the Figs. 4(d,e) due to the strong coupling to the iTO phonon from  $K$  point at 166meV. Here we emphasize that the evaluation of  $\lambda$  from  $\text{Im}(\Sigma)$  does not depend on the details of the dispersion of the bare bands. For the analysis of  $\lambda$  from  $\text{Re}(\Sigma)$  we used the TB calculation of the bare bands which gives the correct curvature in  $KM$  and  $K\Gamma$  directions. Thus our analysis does not suffer from an overestimation of  $\lambda$  in  $KM$  direction. Moreover, from the slope of  $\text{Re}(\Sigma)$  and from the height of the jump in  $\text{Im}(\Sigma)$  it is possible to evaluate the EPC  $\lambda$ <sup>39</sup>: the values we got are  $\lambda = 0.4$  and  $\lambda = 0.3$  from the analysis of  $\text{Re}(\Sigma)$  and  $\text{Im}(\Sigma)$ , respectively. This procedure can be used to obtain the wavevector dependence of  $\lambda_k$ . In Fig. 4(f) we show that the EPC obtained from both the  $\text{Re}(\Sigma)$  (squares) and  $\text{Im}(\Sigma)$  (circles): we thus obtain that  $\lambda_k$  is maximum close to  $KM$  direction and minimum in the  $K\Gamma$  direction. As can be seen in the Fig. 4(f) the resulting  $\lambda$  from  $\text{Re}(\Sigma)$  and  $\text{Im}(\Sigma)$  are in good agreement regarding the anisotropy of the coupling although the actual size of the coupling differs by about 20 %. The minor anisotropy obtained in previous DFT calculations<sup>41</sup> compared to the one extracted from the present work [Fig. 4(f)] and other experimental works<sup>12,40</sup> raises some concerns related to the need of going beyond LDA to describe exchange and correlation effects in the QP energies and wavefunctions. As we stated above, self-energy corrections at the  $GW$  level are needed to describe the observed absence of ARPES intensity at  $\Gamma$ , in contrast to what is predicted by LDA. Another possible explanation to partly explain the strong anisotropy in  $\lambda_k$  observed experimentally might be the phonon trigonal warping effect<sup>42</sup>. Thus further work is

needed to address the phonon dispersion relation and the impact of the  $GW$  self-energy corrections on EPC <sup>38</sup> which we are currently working on. We have also analyzed  $\beta$ , i.e. the coefficient of the quadratic energy dependence of  $\text{Im}(\Sigma)$  which is depicted as crosses in Fig. 4(f) (see also Supplement Fig. 10). Interestingly,  $\lambda$  and  $\beta$  have the same anisotropy, which reflects the anisotropy of the QP bandstructure at  $E_F$ .

The strong EPC limits the maximum bias current through graphene based nanoelectronic devices and is responsible for the strong double-resonance Raman scattering in  $sp^2$  bonded carbon materials. In classical BCS theory, with a pairing mechanism based on EPC it is also one of the limiting factors for the transition temperature of  $KC_8$ . The evaluated transition temperature using the McMillan formula <sup>43</sup> with the high phonon temperature  $\Theta = 1926$  K and the average EPC constant of  $\lambda = 0.45$  [Fig. 4(f)] and a screened pseudopotential  $\mu^* \sim 0.14$  <sup>18</sup> would allow a  $T_C$  up to 6 K. These remaining differences to the experimental  $T_C$  can be explained by either uncertainties in  $\mu^*$  or by additional not yet known pair breaking effects.

In conclusion we have synthesized  $KC_8$  in-situ and performed ARPES measurements. We have found a complete charge transfer and that the QP dispersion of  $KC_8$  is strongly modified in the presence of EPC to the iTO phonon branch at  $K$ . The value of the coupling constant is in good agreement to the experimental value of  $T_C$  and hence determines the superconducting pairing mechanism. Interestingly, this iTO phonon branch is also responsible for the strong double resonance Raman scattering in  $sp^2$  bonded graphite materials. The QP band structure of  $KC_8$  is in good agreement to ab-initio calculations for graphene after including self-energy corrections on a  $GW$

level. We thus conclude that the conical band dispersion of  $\text{KC}_8$  closely resembles that of Dirac Fermions of graphene after applying a gate voltage. Our results circumvent the problems which are associated with strong substrate interaction of graphene<sup>6,33,34</sup> or with interlayer interaction<sup>9</sup>, both of which cause a breakdown of Dirac Fermions. Most importantly, we unravelled for the first time the full experimental Dirac cone of doped graphene and directly determine the corresponding momentum dependent  $v_F$  in the valence and conduction band as such providing crucial input for the understanding of the unique electronic and transport properties of graphene.

## Methods

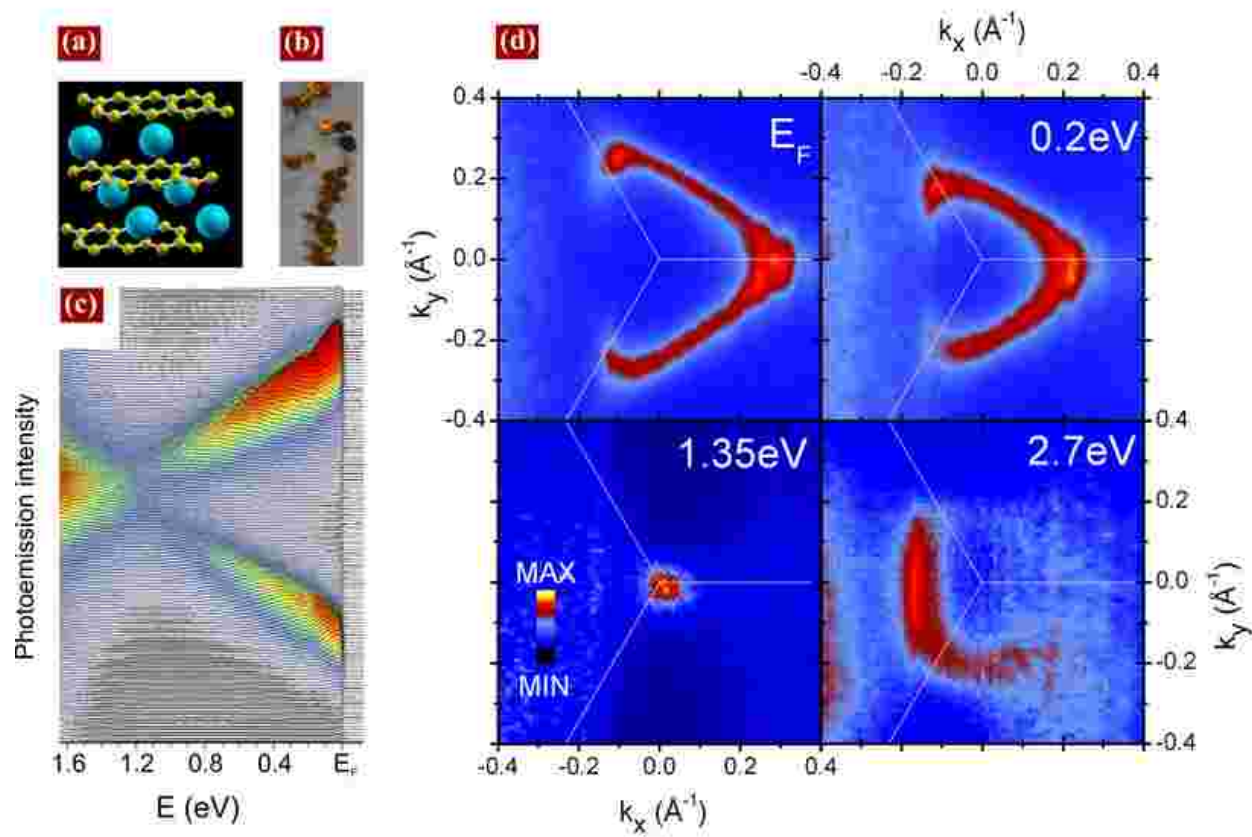
Experiments were done at BESSY II using the UE112-PGM2 beamline and a Scienta RS 4000 analyzer yielding a total energy resolution of 15 meV and a momentum resolution better than  $0.01 \text{ \AA}^{-1}$ . Natural graphite single crystal samples were mounted on a three axis manipulator and cleaved in-situ. Intercalation was performed with the sample at room temperature by evaporating potassium metal from a commercially available SAES getter source. In order to check the doping level, we measured ARPES after each intercalation step. The proof that we reached stage I was given by the appearance of only one  $\pi$  valence band [instead of 2(3) valence bands for stages II(III)]. In addition stage I compounds are identified by their characteristic golden color. After full intercalation,  $\text{KC}_8$  was immediately cooled down by liquid He to 25 K and measured. The calculations of the electronic dispersion of graphene in a slab geometry ( $d = 20 \text{ a.u.}$ ) are performed on two levels. First, we calculate the Kohn-Sham band-structure within the LDA to density-functional theory<sup>44</sup>. Wave functions are expanded in plane waves with an energy cutoff at 25 Ha. Core elec-

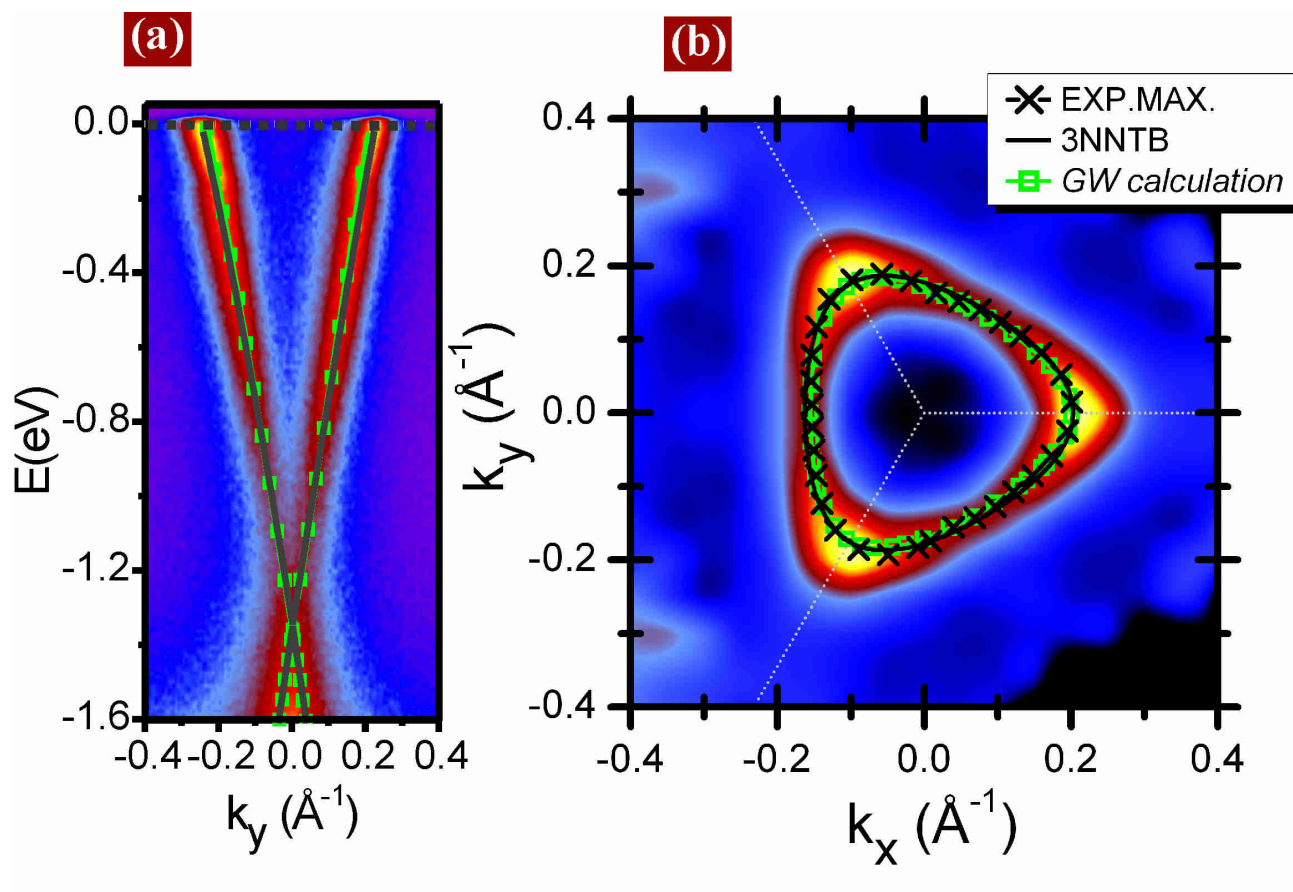
trons are accounted for by Trouiller-Martins pseudopotentials. In the second step, we use the  $GW$  approximation<sup>30–32</sup> to calculate the self-energy corrections to the LDA dispersion<sup>45</sup>. For the calculation of the dielectric function  $\epsilon(\omega, q)$  we use a Monkhorst-Pack  $k$  grid sampling  $36 \times 36 \times 1$  points and bands up to 70eV (namely 50 bands) of the first BZ. In a further step we performed  $GW$  calculations including partial self consistency in  $G$ . Note, that this is a conserving approximation whereas the single shot  $G_0W_0$  is not.

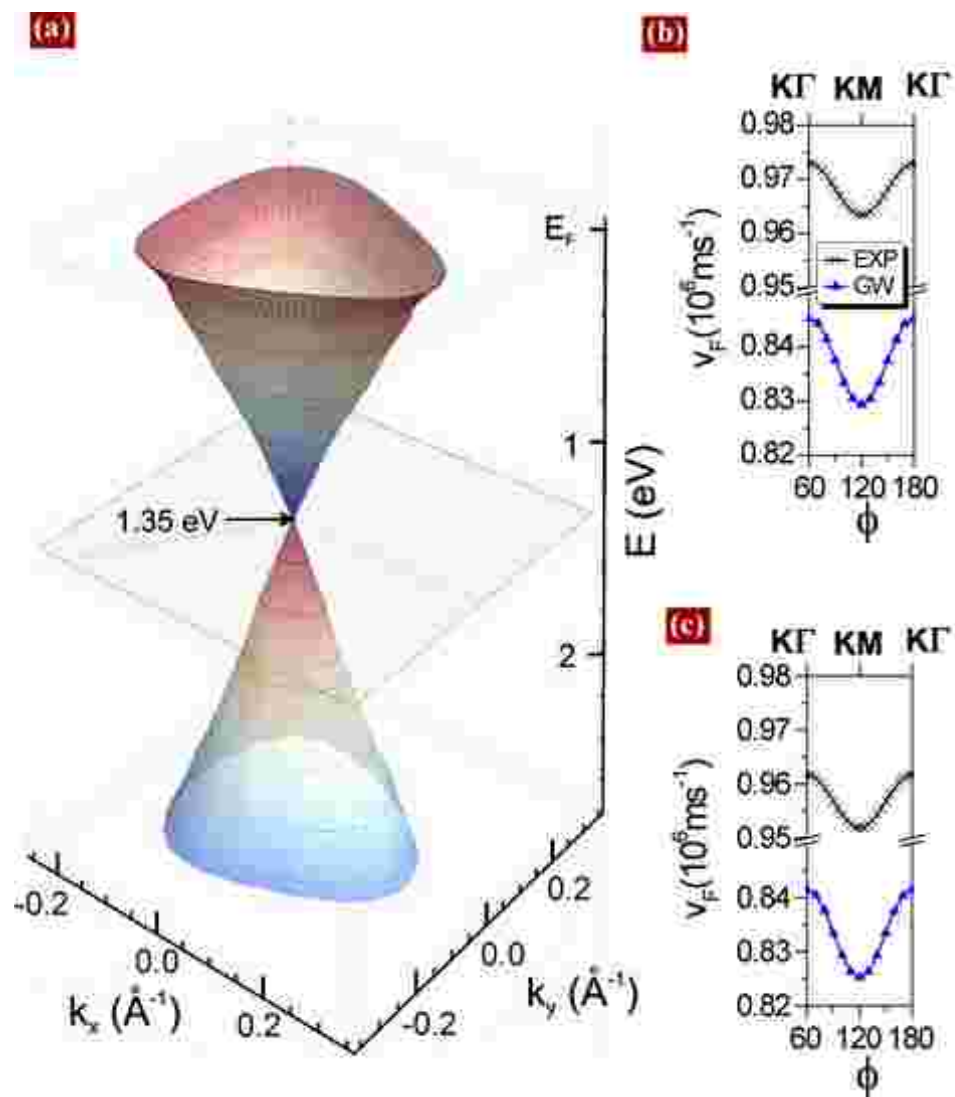
**Acknowledgements** A.G. acknowledges a Marie Curie Individual Fellowship (COMTRANS) from the European Union. T.P. acknowledges DFG projects PI 440/3 and 440/4. C.A. and A.R. acknowledge funding by the Spanish MEC (FIS2007-65702-C02-01), "Grupos Consolidados UPV/EHU del Gobierno Vasco" (IT-319-07), and by the European Community through NoE Nanoquanta (NMP4-CT-2004-500198), e-I3 ETSF project (INFRA-2007-1.2.2: Grant Agreement Number 211956) SANES(NMP4-CT-2006-017310), DNA-NANODEVICES (IST-2006-029192) and NANO-ERA Chemistry projects and the computer resources provided by the Barcelona Supercomputing Center, the Basque Country University UPV/EHU (SGIker Arina).

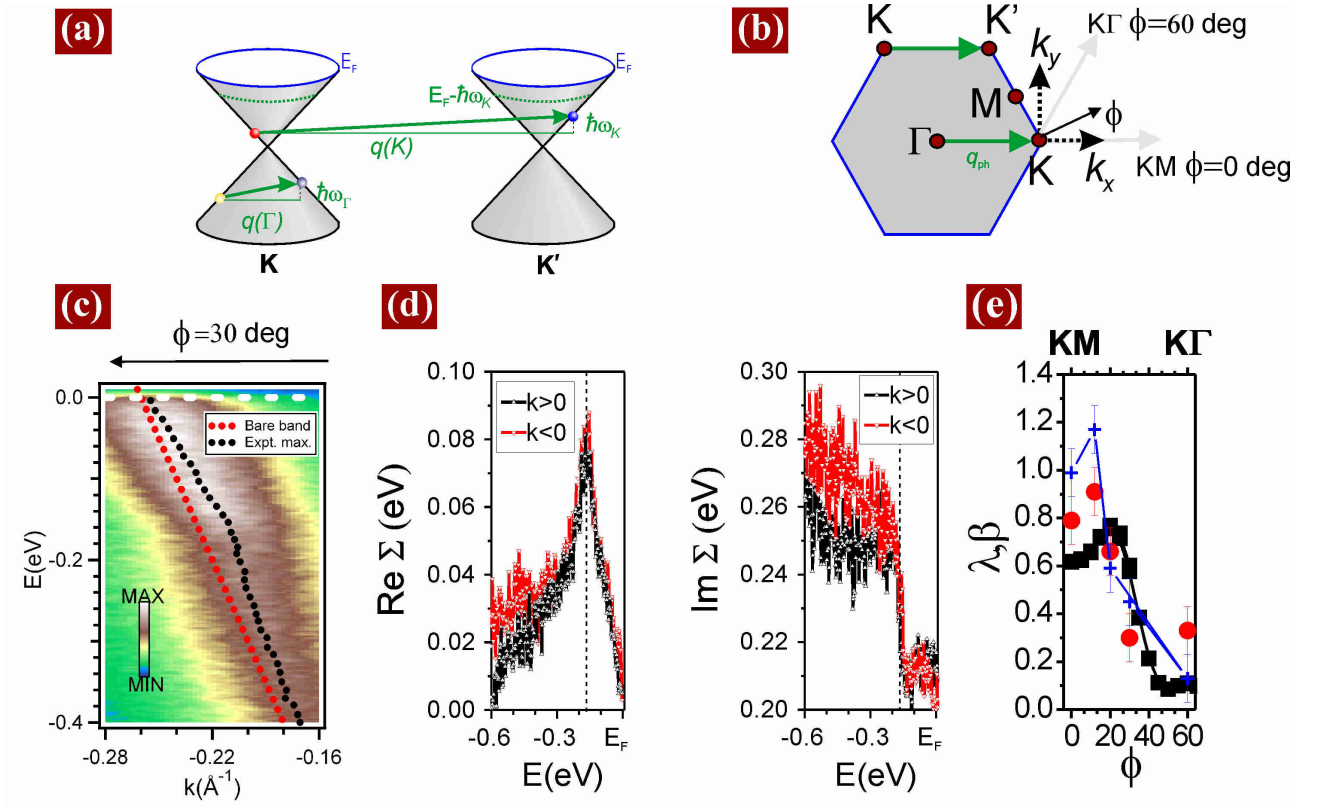
**Competing Interests** The authors declare that they have no competing financial interests.

**Correspondence** Correspondence and requests for materials should be addressed to A. G. (email: ag3@biela.ifw-dresden.de).









1. Geim, A. & Novoselov, K. The rise of graphene. *Nature Mat.* **6**, 183 (2007).
2. Pichler, T. Molecular nanostructures: Carbon ahead. *Nature Mat.* **6**, 332 (2007).
3. Novoselov, K., Geim, A., Morozov, S., Jiang, D., Zhang, Y., Dubonos, S., Grigorieva, I. & Firsov, A. Electric field effect in atomically thin carbon films. *Science* **306**, 666 (2004).
4. Zhou, S. Y., Gweon, G. H., Graf, J., Fedorov, A. V., Spataru, C. D., Diehl, R. D., Kopelevich, Y., Lee, D. H., Louie, S. G. & Lanzara, A. Direct observation of dirac fermions in graphite. *Nature Phys.* **69**, 245419 (2006).



5. Nagashima, A., Tejima, N. & Oshima, C. Electronic states of the pristine and alkali-metal-intercalated monolayer graphite/Ni(111) systems. *Phys. Rev. B* **50**, 17487 – 17495 (1994).
6. Grüneis, A. & Vyalikh, D. Tunable hybridization of electronic states of graphene and metal surfaces. *Phys. Rev. B* **77**, 193401 (2008).
7. Seyller, T., Emtsev, K., Gao, K., Speck, F., Ley, L., Tadich, A., Broekman, L., Riley, J., Leckey, R., Rader, O., Varykhalov, A. & Shikin, A. Structural and electronic properties of graphite layers grown on SiC(0001). *Surf. Sci.* **600**, 3906 (2006).
8. Ohta, T., Bostwick, A., Seyller, T., Horn, K. & Rotenberg, E. Controlling the electronic structure of bilayer graphene. *Science* **313**, 951 (2006).
9. Grüneis, A., Attaccalite, C., Pichler, T., Zabolotnyy, V., Shiozawa, H., Molodtsov, S., Inosov, D., Koitzsch, A., Knupfer, M., Schiessling, J., Follath, R., Weber, R., Rudolf, P., Wirtz, L. & Rubio, A. Electron–electron correlation in graphite: A combined angle-resolved photoemission and first-principles study. *Phys. Rev. Lett.* **100**, 037601 (2008).
10. Sugawara, K., Sato, T., Souma, S., Takahashi, T. & Suematsu, H. Anomalous quasiparticle lifetime and strong electron-phonon coupling in graphite. *Phys. Rev. Lett.* **98**, 036801 (2007).
11. Orlita, M., Faugeras, C., Martinez, G., Maude, D., Sadowski, M. & Potemski, M. Dirac fermions at the H point of graphite: Magnetotransmission studies. *Phys. Rev. Lett.* **100**, 136403 (2008).

12. McChesney, J., Bostwick, A., Ohta, T., Emtsev, K., Seyller, T., Horn, K. & Rotenberg, E. Massive enhancement of electron-phonon coupling in doped graphene by an electronic singularity. *cond-mat* 0705.3264 (2007).
13. Bostwick, A., Ohta, T., Seyller, T., Horn, K. & Rotenberg, E. Experimental determination of the spectral function of graphene. *Nature Phys.* **3**, 36 (2007).
14. Dresselhaus, M. S. & Dresselhaus, G. Intercalation compounds of graphite. *Advances in Phys.* **30**, 139 (1981).
15. Hannay, N., Geballe, T., Matthias, B., Andres, K., Schmidt, P. & MacNair, D. Superconductivity in graphitic compounds. *Phys. Rev. Lett.* **14**, 225 (1965).
16. Csanyi, G., Littlewood, P. B., Nevidomskyy, A. H., Pickard, C. & Simons, B. The role of the interlayer state in the electronic structure of superconducting graphite intercalated compounds. *Nature Physics* **1**, 42 (2005).
17. Sasaki, K., Jiang, J., Saito, R., Onari, S. & Tanaka, Y. Theory of superconductivity of carbon nanotubes and graphene. *J. Phys. Soc. Jpn.* **76**, 033702 (2007).
18. Calandra, M. & Mauri, F. Theoretical Explanation of Superconductivity in  $C_6Ca$ . *Phys. Rev. Lett.* **95**, 237002 (2005).
19. Blinkowski, J., Hau, N., Rigaux, C., Vieren, J., Toullec, R., Furdin, G., Herold, A. & Melin, J. Band structure model and dynamical dielectric function in lowest stage graphite acceptor compounds. *J. Physique* **41**, 47 (1980).

20. Saito, R. & Kamimura, H. Orbital susceptibility of higher-stage graphite intercalation compounds. *Phys. Rev. B* **33**, 7218 (1986).
21. Rytkönen, K., Akola, J. & Manninen, M. Density functional study of alkali metal atoms and monolayers on graphite. *Phys. Rev. B* **75**, 075401 (2007).
22. Eberhardt, W., McGovern, I., Plummer, E. & Fisher, J. Charge-transfer and non-rigid-band effects in the graphite compound  $\text{LiC}_6$ . *Phys. Rev. Lett.* **44**, 200 (1980).
23. N.Gunasekara & T.Takahashi. Angle resolved photomission of first stage alkali metal intercalation compounds. *Condensed Matter* **70**, 349 (1988).
24. Wang, G., Datars, W. & Ummat, P. Band structure and charge transfer of the stage-2 potassium intercalation compound. *Phys. Rev. B* **44**, 10880 (1991).
25. Johnson, M., Starnberg, H. & Hughes, H. Electronic structure of ordered Cs and K overlayers on graphite: observation of complete charge transfer. *Solid State Commun.* **57**, 545 (1986).
26. Algdal, J., Balasubramanian, T., Breitholtz, M., Kihlgren, T. & Wallden, L. Thin graphite overlayer: graphene and alkali metal intercalation. *Surface Science* **61**, 1167 (2007).
27. Zhang, J. M. & Eklund. Optical transmission of graphite and potassium graphite intercalation compounds. *J.Mat.Res.* **2**, 858 (1987).
28. Oelhafen, P., Pfluger, P., Hauser, E. & Günterodt, H. Evidence for an alkali like conduction band in alkali graphite intercalation compound. *Phys. Rev. Lett.* **44**, 197 (1980).

29. Roldan, R., Lopez-Sancho, M. & Guinea, F. Effect of electron-electron interaction on the fermi surface topology of doped graphene. *Phys. Rev. B* **77**, 115410 (2008).
30. Hybertsen, M. S. & Louie, S. G. Electron correlation in semiconductors and insulators: Band gaps and quasiparticle energies. *Phys. Rev. B* **34**, 5390 (1986).
31. Hedin, L. New method for calculating the one-particle green's function with application to the electron-gas problem. *Phys. Rev.* **139**, A796–A823 (1965).
32. Louie, S. G. *Topics in Computational Materials Science*, edited by C. Y. Fong (World Scientific, Singapore) 96 (1997).
33. Zhou, S., Gweon, G., Fedorov, A., First, P., de Heer, W., Lee, D., Guinea, F., Neto, A. H. C. & Lanzara, A. Substrate-induced bandgap opening in epitaxial graphene. *Nature Mat.* **6**, 916 (2007).
34. Zhou, S., Siegel, D., Fedorov, A., Gabaly, F., Schmid, A., Neto, A. C., Lee, D.-H. & Lanzara, A. Origin of the energy bandgap in epitaxial graphene - reply. *Nature Mat.* **7**, 259 (2008).
35. Grüneis, A., Saito, R., Kimura, T., Cançado, L. G., Pimenta, M. A., Jorio, A., Souza Filho, A. G., Dresselhaus, G. & Dresselhaus, M. S. Determination of two-dimensional phonon dispersion relation of graphite by Raman spectroscopy. *Phys. Rev. B* **65**, 155405 (2002).
36. Wirtz, L. & Rubio, A. The phonon dispersion of graphite revisited. *Solid State Comm.* **131**, 141 (2004).

37. Maultzsch, J., Reich, S., Thomsen, C., Requardt, H. & Ordeon, P. Phonon dispersion of graphite. *Phys. Rev. Lett.* **92**, 75501 (2004).
38. Basko, D. & Aleiner, I. Interplay of coulomb and electron-phonon interactions in graphene. *Phys. Rev. B* **77**, 041409 (2008).
39. Fink, J., Koitzsch, A., Geck, J., Zabolotnyy, V., Knupfer, M., Büchner, B., Chubukov, A. & Berger, H. Reevaluation of the coupling to a bosonic mode of the charge carriers in  $(\text{Bi,Pb})_2\text{Sr}_2\text{CaCu}_2\text{O}_{8+\delta}$  at the antinodal point. *Phys. Rev. B* **74**, 165102 (2004).
40. Valla, T., Camacho, J., Pan, Z.-H., Fedorov, A., Walters, A., Howard, C. & Ellerby, M. Anisotropic electron-phonon coupling and dynamical nesting on the graphene sheets in  $\text{CaC}_6$ . *arXiv:0803.0254* (2008).
41. Park, C., Giustino, F., McChesney, J., Bostwick, A., Ohta, T., Rotenberg, E., Cohen, M. & Louie, S. Van hove singularity and apparent anisotropy in the electron-phonon interaction in graphene. *Phys. Rev. B* **77**, 113410 (2008).
42. Samsonidze, G. G., Saito, R., Jorio, A., Souza Filho, A. G., Grüneis, A., Pimenta, M. A., Dresselhaus, G. & Dresselhaus, M. S. Phonon trigonal warping effect in graphite and carbon nanotubes. *Phys. Rev. Lett.* **90**, 027403 (2003).
43. McMillan, W. Transition temperature of strong coupled superconductors. *Phys. Rev.* **167**, 331 (1968).

44. Gonze, X., Beuken, J., Caracas, R., Detraux, F., Fuchs, M., Rignanese, G., Sindic, L., Verstraete, M., Zerah, G., Jollet, F., Torrent, M., Roy, A., Mikami, M., Ghosez, P., Raty, J. & Allan, D. *Comput. Mater. Sci.* 478 (2002).
45. A. Marini et al., the Yambo project, <http://www.yambo-code.org/>.

**Figure 1** (a) Crystal structure of  $\text{KC}_8$ . (b) Photo of intercalated  $\text{KC}_8$  single crystals with golden colour. (c) As measured EDC cuts through the corner of the 3D BZ. (d) Equi-energy contours of the photoemission intensity taken at 48 eV photon energy for four binding energies.

**Figure 2** (a) ARPES scan measured close to the  $k_y$  direction along with the TB fit of the bare-band dispersion (black) and the  $GW$  calculation for electrostatically doped graphene (blue) and undoped graphene (green circles). (b) Symmetrized equi-energy contour for  $E=0.24$  eV and maxima (crosses) along with the TB fit and the  $GW$  ab-initio calculations.

**Figure 3** (a) Experimental Dirac cone from the observed photoemission intensity maxima (denoted as dots). Measured and calculated ( $GW$ ) values of  $v_F$  for (b) electrons and (c) holes around the Dirac point.

**Figure 4** (a) Schematics of the photohole scattering process from  $K$  to  $K'$  by EPC to a  $K$  point phonon with energy  $\hbar\omega_{ph}(q_{ph})$ . The initial and final photohole states around  $K$  and  $K'$  are denoted by circles. The arrow denotes the exchanged phonon with wavevector  $q_{ph}$  and energy  $\hbar\omega_{ph}(q_{ph})$  which is emitted by photohole relaxation. (b) 2D BZ indicating the phonon wavevector  $q_{ph}$ . (c) measured ARPES intensity in the region of the kink. A straight dashed line denotes the bare band dispersion and a kinked dotted line are the experimental MDC maxima. (d) real and (e) imaginary part of the self-energy. (f) the angular dependence of the EPC constant  $\lambda$  and the electron-electron correlation constant

$\beta$ ; black squares(red circles) denote  $\lambda$  extracted from the measured real(imaginary) part of the self-energy.  $\beta$  is denoted by blue crosses.